The Contributions of Shear and Turbulence to Cloud Overlap for Cumulus Clouds

Anthony Sulak[1,2], **William Calabrase**[1,3], **Shawn D. Ryan**[1], **and Thijs Heus**[1]

[1]Cleveland State University, Cleveland, OH
[2]Michigan State University, East Lansing, MI
[3]Case Western Reserve University, Cleveland, OH

Key Points:

- Cloud Overlap of individual cumulus clouds is a good representation of the entire cloud field
- Explicitly including shear and turbulence yields a strong improvement over maximum overlap alone
- We develop a conceptual model that represents overlap well

Corresponding author: Thijs Heus, `t.heus@csuohio.edu`

Abstract

Vertical cloud overlap, the ratio of cloud fraction by area and by volume, for cumulus clouds are studied using large-eddy simulations (LES) due to the inefficient, wide-range values of cloud overlap. We can obtain information about the cloud cover of a cloud field by inspecting the individual clouds in that cloud field. We start with the maximum-random assumption and adjust this assumption for individual clouds. From this there is an underprediction which leads to the conclusion that something can be added. We extend this by considering physical factors of cloud overlap: area variability, vertical wind shear, and turbulence. We use numerical schemes to calculate the effect of each contributor based on cloud height. We obtain great accuracy for our model of cloud overlap. Since there are multiple factors of cloud overlap, we look at the percentage of how much each contributes for a given binned cloud height. Furthermore, we get acceptable agreement for the calculated and actual total cloud cover. As such, we show that no other major contributors for cloud overlap and cloud cover exist. We end with an empirical model to describe the numerical schemes mentioned previously.

1 Introduction

Clouds are a challenging component of the atmosphere to model (Bony et al., 2015). This is particularly true as we enter the grey zone of convection (Honnert, Masson, & Couvreux, 2011; Wyngaard, 2004), where some convection is resolved, but smaller clouds still need to be represented in the subgrid parameterization. One approach to resolve this problem is to formulate the convection parameterization as a function of cloud size (e.g., Neggers, 2015; Plant & Craig, 2008; Sakradzija, Seifert, & Heus, 2015). So far, these parameterizations have mainly focused on transport instead of other components of cloud parameterizations, such as precipitation and radiation.

Cloud overlap is an important component of the parameterization of cloud fields, for two reasons: First, the way clouds and cloud fields are stacked has significant impact on the cloud cover, and hence on radiation (e.g., Hogan & Illingworth, 2000). This is especially true for shallow cumulus clouds, whose small cloud size limits the effect of the zenith angle on the cloud cover (Kleiss et al., 2018), although in-cloud inhomogeneity of liquid water tends to counteract the overlap effect a bit. Second, overlap impacts the formation of precipitation (Ovchinnikov, Giangrande, Larson, Protat, & Williams, 2019), and cumulus clouds are often on the verge of precipitating or not (Seifert & Stevens, 2010). Park (2017, 2018) found a significant impact of the overlap parameterization on both the precipitation and the radiation effects of boundary layer clouds. Previous work on cloud overlap has focused mostly on the overlap between cloud layers, (e.g., Barker, 2008; Geleyn & Hollingsworth, 1979; Hogan & Illingworth, 2000), or on deep convective systems (e.g., Oreopoulos & Khairoutdinov, 2003; Pincus, Hannay, & Evans, 2005), but recently the significance of overlap in shallow convection has also been recognized. Previous work also found that Large Eddy Simulations (LES) are able to generate cloud fields with an overlap ratio that compares well with observations (Corbetta, Orlandi, Heus, Neggers, & Crewell, 2015), and that cloud fields tend to be a lot less efficiently stacked than previously assumed (Neggers, Heus, & Siebesma, 2011). This efficiency was expressed by Hogan and Illingworth (2000) using a decorrelation length Δz_0, which measures the depth beyond which layers are no longer perfectly stacked (maximum overlap, c_{max}), but shows no correlation in placement anymore, resulting in a random overlap *(c_{rand})*:

$$c_p = \alpha c_{max} + (1 - \alpha) c_{rand} \tag{1}$$

with c_p the projected cloud cover, α an overlap parameter, characterized for instance as an exponential decay as a function of layer depth Δz:

$$\alpha = \exp\left(-\frac{\Delta z}{\Delta z_0}\right) \tag{2}$$

Neggers et al. (2011) found a decorrelation length around 300m, much smaller than the multiple kilometer range that previous studies on deep convection found.

An alternative formulation (Brooks, Hogan, & Illingworth, 2005; Del Genio, Yao, Kovari, & Lo, 1996) describes the overlap as a ratio between the projected cloud cover and the average cloud fraction in a layer Δz:

$$r = \frac{c_v}{c_p}. \tag{3}$$

r, which ranges between 0 and 1, then becomes the quantity to parameterize. This formulation is attractive, since c_v is typically available in a convection parameterization. For size dependent schemes like Neggers (2015), this is also true as a function of cloud size. Within this formulation, Neggers et al. (2011) found that overlap is well represented by a ratio:

$$c_p = r^{-1} c_v = (1 + \beta \Delta z)^{-1} c_v \tag{4}$$

with $\beta \approx (160m)^{-1}$, a tuning parameter. Such a formulation also makes intuitive sense, since the minimum possible value for r^{-1} is equal to one, and any irregularity in the cloud field adds to that, be it linear or not.

Tuning parameters like Δz_0 and β are likely case dependent. It therefore makes sense to zoom in on what causes inefficient overlap in a contiguous field of clouds. Likely candidates include (see also Fig. 1):

1. Differences in cloud location and cloud height between clouds. For instance, clouds with different locations of their maximum cloud fraction result in a less-than-maximum overlap. The same is true for variations in cloud top height, where the smaller clouds may not fully pierce through a complete grid box (See Figure 1 in Neggers et al. (2011)).
2. Cloud 'shape', or a cloud width that is not constant with height. An obvious example would be cloud anvils/outflow regions for deeper convection; for shallow cumulus, clouds tend to be widest at cloud base. This is the part that is typically represented by maximum overlap.
3. Wind shear may tilt clouds, affecting the overlap even for constant cloud fraction.
4. Random turbulence yields fractal surfaces for clouds (e.g., Siebesma & Jonker, 2000), which generates overlap inefficiencies as well.

In this paper, we will work towards a physics-based parameterization of overlap by exploring the contributions of the different processes mentioned above. Of these effects, all but the first one is a function of individual cloud shape, and potentially a function of cloud size. We will use LES to explore a variety of cases, although, as we will see, the results are reasonably independent of case. We will then develop a simple parameterization for cloud overlap based on our findings. The outline of the paper is as follows: First, we will briefly discuss the methods used, including the LES code and the cases used. Then, we will assess the contributions of each process mentioned above, and provide a parameterization for them. Finally, we will evaluate the aggregate overlap and its parameterization: We will discuss the relative size of each effect, and the accuracy of the entire parameterization. We will conclude with a brief discussion of overall impact, merits, and future work.

2 Methodology

We are basing our analysis on cloud fields generated with MicroHH (van Heerwaarden et al., 2017). This modern, fast Large Eddy Simulation model has been validated against a wide range of standard cases, including all the intercomparison cases used in this study: BOMEX (Siebesma et al., 2003), which are non-precipitating marine clouds,

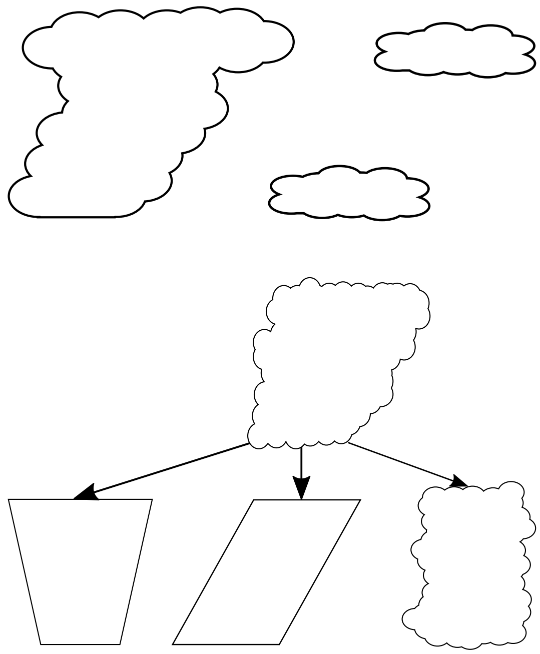

Figure 1. Schematic illustration of different causes of overlap. Top: Overlap due to different cloud locations. Bottom, from left to right: Overlap due to non-constant width, shear, and turbulence.

ARM-SGP (Brown et al., 2002) a diurnal cycle over land, and RICO (vanZanten et al., 2011), somewhat deeper and precipitating marine clouds. Further, we are using a subset of the Large-Eddy Simulation (LES) ARM Symbiotic Simulation and Observation (LASSO; Gustafson et al., 2017) database. These are realistic and routine simulations of cumulus fields over the ARM-Southern Great Planes observatory in Oklahoma. From this LASSO database, we included 10 days from 2016 in the current study and selected the configurations with the best match to the observations in cloud cover and liquid water path. Since the simulations in the LASSO database were done on a relatively coarse resolution of 100m, we re-ran all cases with MicroHH, on a higher resolution.

We simulated all cases using the forcing and settings as described in the respective case description papers. Each simulation was run on a 25m resolution in both the horizontal and vertical direction, with a horizontal domain size of $25km^2$. For BOMEX, we simulated 10 hours, and discarded the first 3 as spin up. Since BOMEX is a steady state case, the final 7 hours are aggregated in our analysis. For RICO, we simulated 60 hours, which allows the cloud field to deepen significantly (cloud top = 3600) and organize (Seifert & Heus, 2013).

As we will see, the results are applicable to all of the cases mentioned above. We will therefore focus on the 8th hour of RICO in the discussion below of the individual effects, and will use the other cases to evaluate the resulting overlap model in section 6.

To quantify the contribution of various effects on the cloud overlap, we calculate and then model the inverse overlap ratio r^{-1} for every process. Ignoring non-linear interactions, these contributions then add up to the total inverse overlap:

$$r_{tot}^{-1} = r_{fld}^{-1} + r_{shape}^{-1} + r_{shr}^{-1} + r_{turb}^{-1} \tag{5}$$

with the terms on the righthand side referring to the contributions of overlap inefficiencies of the cloud field, mean area fluctuations with height, influence of shear, and the effect of turbulence, respectively.

3 Overlap of individual clouds versus cloud fields

Before we can assess the contributions to the overlap of cloud geometry, we first need to study the relative contributions of the intra-cloud and inter-cloud inefficiencies to the cloud overlap. For this, we calculate the inverse overlap for each cloud n:

$$r_{tot}^{-1}(n) = \frac{A_{proj}(n)h(n)}{V(n)}, \tag{6}$$

with A_{proj} the projected area, h the height of, and V the volume of each cloud. In Fig. 2, we show the relationship between the cloud overlap of individual clouds as a function of their height, versus the cloud overlap in that cloud field as a function of layer thickness. While we clearly see a strong correlation between the two, the relationship is not one-to-one. This can mostly be attributed to the variability in cloud height: If smaller clouds only partially fill a cloud layer, the average cloud fraction by volume c_v decreases relative to the projected cloud fraction by area c_p. To quantify this effect, we need to estimate the cloud area as a function of the height distribution. This is a work in progress by the authors, but beyond the scope of the current paper.

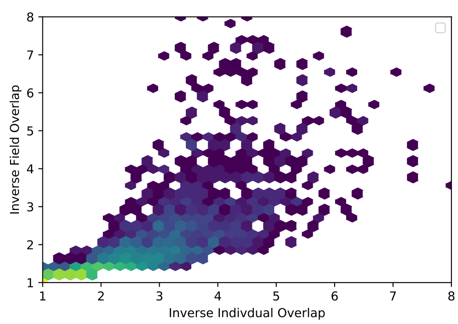

Figure 2. Inverse overlap of the cloud field as a function of layer depth against the inverse overlap of individual clouds of a particular height.

4 Contributions to Individual Cloud Overlap

The next step is to quantify the various effects on cloud overlap of individual clouds. The inverse overlap is plotted as a function of cloud width (defined as $\sqrt{A_{proj}}$; a different definition would yield similar results) in Fig. 3a; it is plotted as a function of cloud height in Fig. 3b. We observe that an inverse overlap of 5 or beyond is possible, especially for the larger clouds. We also observe a clear linear relationshop between size and inverse overlap. However, the correlation between r_{tot}^{-1} and cloud *height* is clearly higher ($R > 0.95$) then the correlation with cloud *width* ($R \approx 0.74$). We will therefore express our overlap relations as a function of cloud height. While this could seemingly complicate a parameterization of overlap as a function of cloud size, it will likely actually help: Most spectral macrophysical models (Neggers, 2015, e.g.,) are expressed as a cloud *core* width; this in turn seems to correlate better with cloud height than with cloud width. The null hypothesis for individual cloud overlap is the limit case of most overlap param-

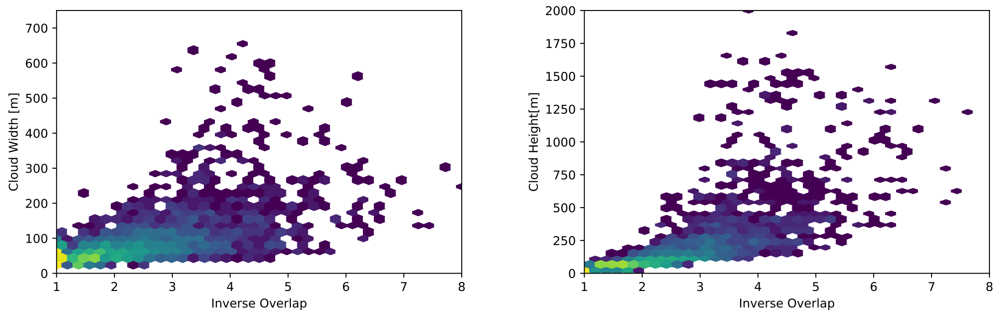

Figure 3. Inverse overlap of individual clouds: a) versus cloud width and b) versus cloud height.

156 eterizations for contiguous clouds, that is, maximum overlap. This can be used to as-
157 sess the mean shape contribution to the individual cloud overlap:

$$r_{shape}^{-1}(n) = \frac{A(n)_{max}}{A(n)_{avg}} - 1, \tag{7}$$

158 where $A(n)_{max}$ is the maximum area of cloud n, and $A(n)_{avg}$ the average area across
159 its height. We subtract 1 to retrieve the effect of maximum overlap beyond the theoret-
160 ical minimum.

161 To quantify the influence of shear, we realign each cloud so that its center of mass
162 as a function of height is constant (see Fig. 4). The effect of shear can then be estimated
163 as the difference between the original inverse overlap and the inverse overlap of the re-
aligned cloud. Finally, the effect of turbulence is estimated by creating a convex hull around

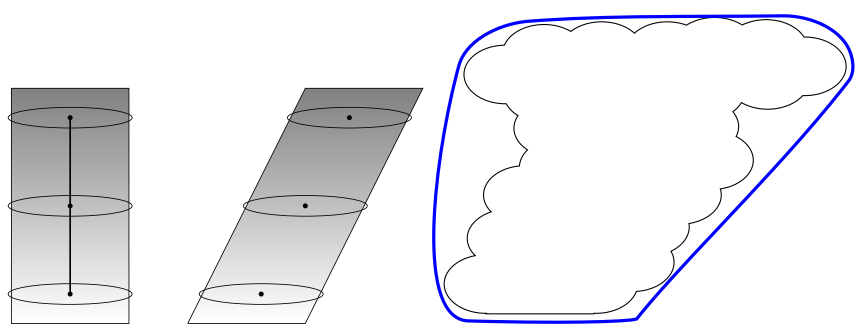

Figure 4. Schematic overview of the method to estimate a) the shear contribution and b) the turbulence contribution to the inverse overlap.

164
165 each cloud (see Fig. 4), and take the difference in overlap between that hull and the orig-
166 inal cloud. This is a rough estimate of the effect of turbulence, and likely an overesti-
167 mation: A cloud with significant concave features (e.g., anvils) would result in spuriously
168 added volume to the hull, without an increase in the projected cloud cover.

169 Fig. 5 plots the actual inverse overlap of each cloud against the cloud inverse over-
170 lap with only the contributions of shape (panel a), shear (b), and turbulence (c). From
171 the figure it is clear that a maximum overlap assumption underestimates the inverse over-
172 lap by a factor of 2, and that all effects contribute significantly to the cloud overlap. Taken

together (panel e), it is clear that the sum of the effects overestimates the actual inverse overlap. This is likely due to double counting in the convex hull estimation of the turbulence. However, a model that only includes shape and shear has a clear bias to underestimate the actual inverse overlap. Some contribution of turbulence remains necessary.

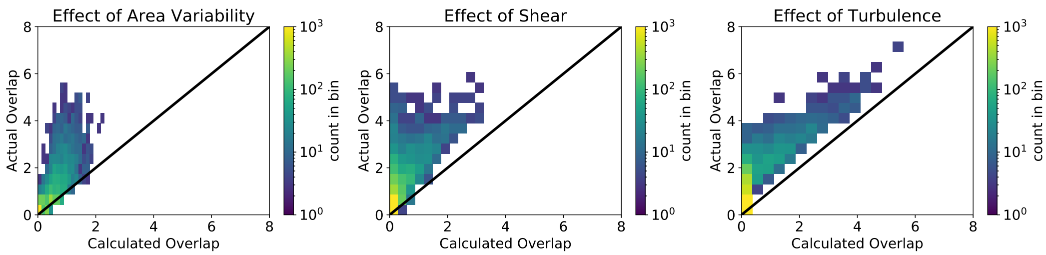

Figure 5. Actual inverse overlap of individual clouds vs the estimated contributions of a) shape, b) shear, and c) turbulence.

5 Parameterization of shear and turbulence

While our cloud shape model is already expressed as a function of large scale parameters, the same is not true for shear or turbulence. For shear, a simple model based on a cylinder tilted due to shear (Fig. 6; see also Neggers et al., 2011) relates the inverse overlap to the updraft speed w and the shear across the cloud Δu:

$$r_{shear}^{-1} = \frac{b}{l} = \frac{h\Delta u}{lw}, \tag{8}$$

with the symbols explained in Fig. 6a. Note that this model assumes constant shear as a function of height, and ignores directional shear. It also assumes a constant updraft speed w, even though there are significant differences between updraft and remnant velocity. From Fig. 6b, it is clear that while the model shows a large spread and can clearly be refined in future work, the average is in line with the observed overlap due to shear.

To develop a model for the turbulence component, we assume that each cloud can be

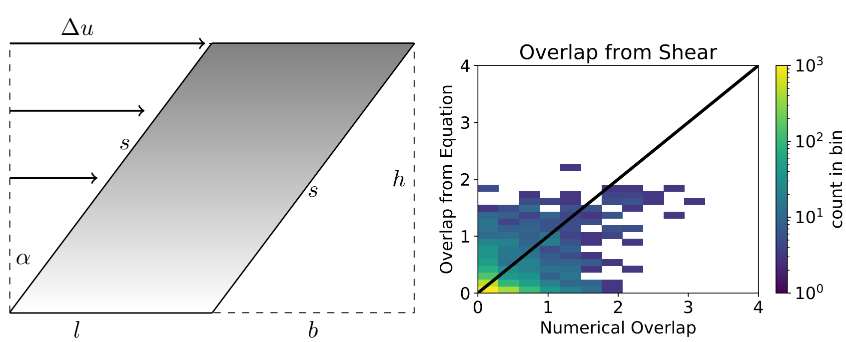

Figure 6. Parameterization of shear-induced overlap: a) Schematic representation; b) Parameterized vs observed shear-induced overlap.

approximated as a fractal, here taken as a 3-dimensional version of a Koch snowflake.

If the cloud is sufficiently deep, the projected cloud cover of the fractal will approach the area of the circumscribing sphere (see Fig. 7a). Since the height of the sphere and the fractal are the same, the inverse overlap is equal to the ratio between the volumes of the fractal and the sphere, which is equal to $\frac{\sqrt{3}\pi}{2}$; see the appendix for a derivation. For smaller clouds, the fractal will not quite saturate the circumscribed sphere, so a decorrelation length scale is appropriate here:

$$r_{turb}^{-1}(h) = \frac{\sqrt{3}\pi}{2} \cdot \frac{h}{h_0 + h} \tag{9}$$

with h_0 the decorrelation length, empirically estimated as 200m. Note that we use the ratio of the *volumes* in this exercise, and not the ratio of the projected areas; this is to avoid double counting with the shape effect. The results are shown in Fig. 7b. Like with the shear model, while there is a significant spread around the curve, the model tends to capture the overall behavior reasonably well.

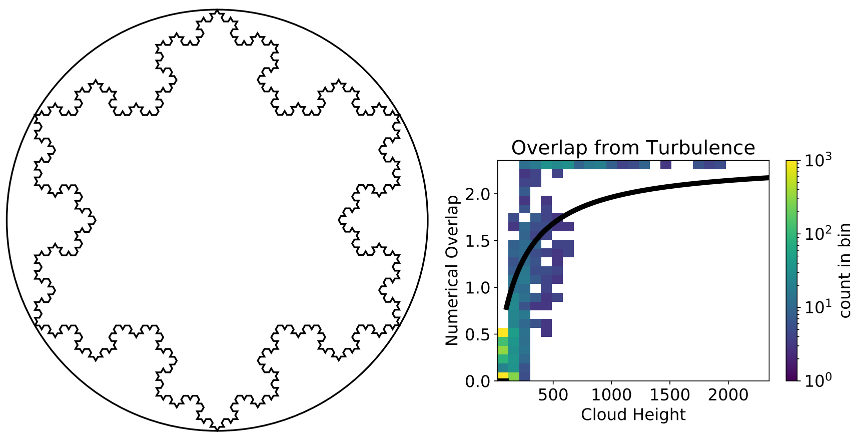

Figure 7. Parameterization of turbulence-induced overlap: a) schematic representation of a 2D-Koch snowflake and its circumscribed circle; b) Parameterized vs observed turbulence-induced overlap.

5.1 Combined

Finally, Fig. 8 shows the skill of the model in three different ways, for four different cases: The top row shows the observed vs. predicted inverse overlap for each cloud; the middle row shows the contribution of each component to the overall inverse overlap as a function of cloud size, and the bottom row shows a histogram of the relative error in predicted inverse overlap. From these graphs, we see consistently good behavior of the model, with a predicted inverse overlap within 10% of the correct value for more than 80% of the clouds, and a small bias towards underpredicting. We also see that, while different from case to case and size to size, all three components contribute significantly to the inverse overlap, and a maximum overlap assumption can only explain less than a third of the inverse overlap, independent of cloud size. Turbulence is a consistently strong contributor, which is good news as it has a mostly scale independent parameterization with only the saturation depth h_0 as a parameter.

6 Discussion and Conclusions

In this study, we presented a model for the cloud overlap of cumulus convection. We show that the overlap is dominated by the overlap within each cloud; the cloud over-

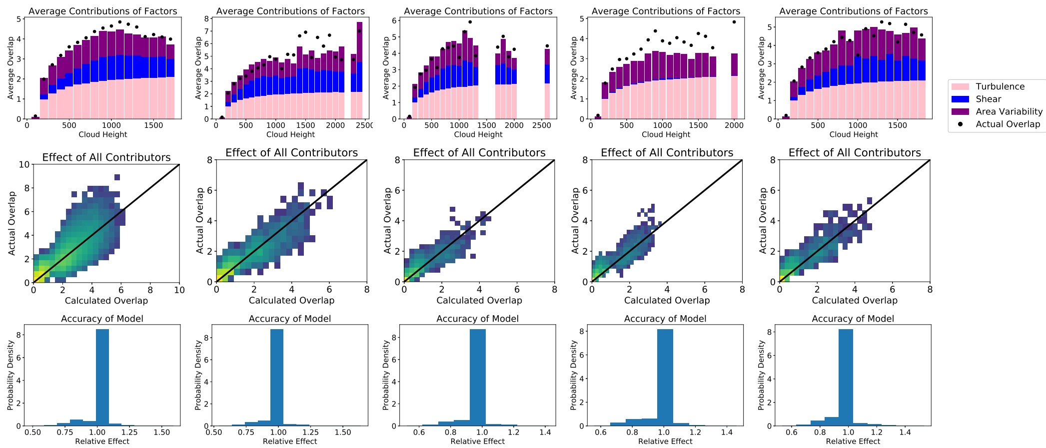

Figure 8. Overall results of the entire parameterization for (left to right): BOMEX, RICO at 8 hrs, RICO at 60 hrs, ARM at 8hrs, and ARM at 11 hrs. Top to bottom: Contributions as a function of cloud width, overall predicted inverse overlap, and distribution of accuracy.

lap between different clouds is of secondary importance. For the intra-cloud overlap, we distinguish three components (shape, shear, and turbulence), each of which has a significant contribution. Our empirical model of these effects is able to predict the cloud overlap very well for a variety of cumulus cases, which gives confidence that the model has some generic applicability. Also, our turbulence model can be modeled as a linear inverse overlap with a decorrelation length of 200m; this matches well with the observationally found value of 160m-590m (Corbetta et al., 2015).

Beyond the cloud overlap, several other factors are to be considered for an accurate description of the radiative impact or of the generated precipitation, and these are areas of interest for future research. First, if our model would be applied directly, the implicit assumption would be that the liquid water content is homogeneous across the cloud. While this is clearly a risky assumption at best, it is likely to hold up better in a bin-macrophysical convection model where the properties of clouds as a function of cloud size are available: With the liquid water content known as a function of cloud size, it is only the variability within each cloud size and within each cloud that needs to be included, as opposed to the much larger variation in liquid water content between clouds of different sizes.

Second, for a radiative model, another missing factor is the solar zenith angle. For very shallow clouds, where the linear horizontal cloud size is much larger than the cloud depth, this is a simple geometric factor; for fields containing deeper clouds the sides will block a significant amount of sunlight as well. According to Kleiss et al. (2018), however, this effect should be minimal for the cloud fields under current consideration.

A The volume of a 3D Koch fractal

A 3D Koch fractal can be generated from a equilateral tetrahedron with rib length s_0, surface area per facet a_0, and volume $v_0 = \frac{s^3}{6\sqrt{2}}$. In each iteration, the facet area of each new tetrahedron is $\frac{1}{4}$ times the previous facet area, so that:

$$a_n = \frac{a_{n-1}}{4} = a_0 \left(\frac{1}{4}\right)^n \qquad \text{(A.1)}$$

$$v_n = \left(\frac{a_n}{a_0}\right)^{\frac{3}{2}} v_0 \tag{A.2}$$

And the number of added tetrahedrons is equal to:

$$T_n = 4 \cdot 6^{n-1} = \frac{2}{3} \cdot 6^n, \tag{A.3}$$

so that the total volume V_n after n iterations is equal to:

$$V_n = v_0 \left(1 + \sum_{j=1}^{n} T_j \left(\frac{1}{4}\right)^{\frac{3j}{2}}\right) = v_0 \left(1 + \frac{1}{2}\sum_{j=1}^{n} \left(\frac{3}{4}\right)^j\right). \tag{A.4}$$

Taking the limit $n \to \infty$ yields:

$$V_\infty = 3v_0 = \frac{s^3}{2\sqrt{2}}. \tag{A.5}$$

The circumsphere of the fractal is the same as the circumsphere of the original tetrahedron, and has a radius $R_{sphere} = \sqrt{\frac{3}{8}}s$, resulting in an inverse overlap ratio of:

$$r_{turb}^{-1} = \frac{V_{sphere}}{V_\infty} = \frac{\frac{4\pi}{3}\left(\frac{3}{8}\right)^{\frac{3}{2}}}{\frac{1}{2\sqrt{2}}} = \frac{\pi\sqrt{3}}{2}. \tag{A.6}$$

Acknowledgments

This research was supported primarily by the U.S. Department of Energy's Atmospheric System Research, an Office of Science, Office of Biological and Environmental Research program, under Grant No. DE-FG02-SC0017999. U.S. Department of Energy as part of the Atmospheric Radiation Measurement (ARM) Climate Research Facility SGP-C1 were used. William Calabrase was funded by CSUs Undergraduate Summer Research Program. The work of Shawn Ryan was supported by the CSU Office of Research. The MicroHH code and all cases are available at `https://github.com/microhh/microhh2`.

References

Barker, H. W. (2008). Representing cloud overlap with an effective decorrelation length: An assessment using cloudsat and calipso data. *Journal of Geophysical Research: Atmospheres*, *113*(D24).

Bony, S., Stevens, B., Frierson, D. M. W., Jakob, C., Kageyama, M., Pincus, R., … Webb, M. J. (2015, March). Clouds, circulation and climate sensitivity. *Nature Geoscience*, *8*, 261–. Retrieved from `https://doi.org/10.1038/ngeo2398`

Brooks, M. E., Hogan, R. J., & Illingworth, A. J. (2005). Parameterizing the Difference in Cloud Fraction Defined by Area and by Volume as Observed with Radar and Lidar. *J. Atmos. Sci.*, *62*, 2248–2260. doi: 10.1175/JAS3467.1

Brown, A. R., Cederwall, R. T., Chlond, A., Duynkerke, P. G., Golaz, J. C., Khairoutdinov, M., … Stevens, B. (2002). Large-eddy simulation of the diurnal cycle of shallow cumulus convection over land. *Quart. J. Roy. Meteor. Soc.*, *128*(582), 1075–1093. doi: 10.1256/003590002320373210

Corbetta, G., Orlandi, E., Heus, T., Neggers, R., & Crewell, S. (2015). Overlap statistics of shallow boundary layer clouds: Comparing ground-based observations with large-eddy simulations. *Geophysical Research Letters*, *42*(19), 8185–8191. Retrieved from `http://dx.doi.org/10.1002/2015GL065140` (2015GL065140) doi: 10.1002/2015GL065140

Del Genio, A. D., Yao, M.-S., Kovari, W., & Lo, K. K. (1996). A prognostic cloud water parameterization for global climate models. *Journal of Climate*, *9*(2), 270– 304.

Geleyn, J., & Hollingsworth, A. (1979). An economical analytical method for the computation of the interaction between scattering and line absorption of radiation. *Contrib. Atmos. Phys.*, *52*.

Gustafson, W., Vogelmann, A., Cheng, X., Endo, S., Johnson, K., Krishna, B., ... Xiao., H. (2017). Atmospheric radiation measurement (arm) research facility. lasso data bundles. southern great plains central facility (c1). *ARM Data Archive: Oak Ridge, Tennessee, USA.*. doi: http://dx.doi.org/10.5439/1342961

Hogan, R. J., & Illingworth, A. J. (2000). Deriving cloud overlap statistics from radar. *Quarterly Journal of the Royal Meteorological Society*, *126*(569), 2903–2909.

Honnert, R., Masson, V., & Couvreux, F. (2011). A diagnostic for evaluating the representation of turbulence in atmospheric models at the kilometric scale. *Journal of the Atmospheric Sciences*, *68*(12), 3112-3131. Retrieved from `https://doi.org/10.1175/JAS-D-11-061.1` doi: 10.1175/JAS-D-11-061.1

Kleiss, J. M., Riley, E. A., Long, C. N., Riihimaki, L. D., Berg, L. K., Morris, V. R., & Kassianov, E. (2018). Cloud area distributions of shallow cumuli: A new method for ground-based images. *Atmosphere*, *9*(7). Retrieved from `https://www.mdpi.com/2073-4433/9/7/258` doi: 10.3390/atmos9070258

Neggers, R. A. J. (2015). Exploring bin-macrophysics models for moist convective transport and clouds. *J. Adv. Model. Earth Syst.*, n/a–n/a. Retrieved from `http://dx.doi.org/10.1002/2015MS000502`

Neggers, R. A. J., Heus, T., & Siebesma, A. P. (2011). Overlap statistics of cumuliform boundary-layer cloud fields in large-eddy simulations. *J. Geophys. Res.*, *116*(D21202).

Oreopoulos, L., & Khairoutdinov, M. (2003). Overlap properties of clouds generated by a cloud-resolving model. *Journal of Geophysical Research: Atmospheres*, *108*(D15). Retrieved from `https://agupubs.onlinelibrary.wiley.com/doi/abs/10.1029/2002JD003329` doi: 10.1029/2002JD003329

Ovchinnikov, M., Giangrande, S., Larson, V. E., Protat, A., & Williams, C. R. (2019, FEB 27). Dependence of Vertical Alignment of Cloud and Precipitation Properties on Their Effective Fall Speeds. *JOURNAL OF GEOPHYSICAL RESEARCH-ATMOSPHERES*, *124*(4), 2079-2093. doi: {10.1029/2018JD029346}

Park, S. (2017, OCT). A Heuristic Parameterization for the Integrated Vertical Overlap of Cumulus and Stratus. *JOURNAL OF ADVANCES IN MODELING EARTH SYSTEMS*, *9*(6), 2437-2465. doi: {10.1002/2017MS001055}

Park, S. (2018, MAR). An Economical Analytical Equation for the Integrated Vertical Overlap of Cumulus and Stratus. *JOURNAL OF ADVANCES IN MODELING EARTH SYSTEMS*, *10*(3), 826-841. doi: {10.1002/2017MS001190}

Pincus, R., Hannay, C., & Evans, K. F. (2005, 7). The accuracy of determining three-dimensional radiative transfer effects in cumulus clouds using ground-based profiling instruments. *J. Atmos. Sci.*, *62*(7), 2284–2293. doi: 10.1175/JAS3464.1

Plant, R. S., & Craig, G. C. (2008, January). A stochastic parameterization for deep convection based on equilibrium statistics. *J. Atmos. Sci.*, *65*(1), 87–105. Retrieved from `http://dx.doi.org/10.1175/2007JAS2263.1` doi: 10.1175/2007JAS2263.1

Sakradzija, M., Seifert, A., & Heus, T. (2015). Fluctuations in a quasi-stationary shallow cumulus cloud ensemble. *Nonlinear Processes in Geophysics*, *22*(1), 65–85. Retrieved from `http://www.nonlin-processes-geophys.net/22/65/2015/npg-22-65-2015.html` doi: 10.5194/npg-22-65-2015

Seifert, A., & Heus, T. (2013). Large-eddy simulation of organized precipitating trade wind cumulus clouds. *Atmospheric Chemistry and Physics*, *13*(1), 5631–5645. Retrieved from `http://www.atmos-chem-phys-discuss.net/13/1855/`

2013/ doi: 10.5194/acpd-13-5631-2013

Seifert, A., & Stevens, B. (2010, May). Microphysical scaling relations in a kinematic model of isolated shallow cumulus clouds. *Journal of the Atmospheric Sciences*, *67*(5), 1575–1590. doi: 10.1175/2009JAS3319.1

Siebesma, A. P., Bretherton, C. S., Brown, A., Chlond, A., Cuxart, J., Duynkerke, P. G., ... Stevens, D. E. (2003). A large eddy simulation intercomparison study of shallow cumulus convection. *J. Atmos. Sci.*, *60*(10), 1201–1219. doi: 10.1175/1520-0469(2003)60

Siebesma, A. P., & Jonker, H. J. J. (2000). Anomalous scaling of cumulus cloud boundaries. *Phys. Rev. Lett.*, *85*, 214–217. doi: 10.1103/PhysRevLett.85.214

van Heerwaarden, C. C., van Stratum, B. J. H., Heus, T., Gibbs, J. A., Fedorovich, E., & Mellado, J. P. (2017). Microhh 1.0: a computational fluid dynamics code for direct numerical simulation and large-eddy simulation of atmospheric boundary layer flows. *Geoscientific Model Development*, *10*(8), 3145–3165. Retrieved from https://www.geosci-model-dev.net/10/3145/2017/ doi: 10.5194/gmd-10-3145-2017

vanZanten, M. C., Stevens, B., Nuijens, L., Siebesma, A. P., Ackerman, A. S., Burnet, F., ... Wyszogrodzki, A. (2011). Controls on precipitation and cloudiness in simulations of trade-wind cumulus as observed during rico. *Journal of Advances in Modeling Earth Systems*, *3*(2), M06001. Retrieved from http://dx.doi.org/10.1029/2011MS000056 doi: 10.1029/2011MS000056

Wyngaard, J. (2004). Toward numerical modeling in the "Terra Incognita". *Journal of the Atmospheric Sciences*, *61*, 1816–1826. doi: 10.1175/1520-0469(2004)061